Tikrit Journal of Engineering Sciences

TJES Tikrit Journal of Engineering Sciences

Open Access

Article

Use of ZSM-5 Photocatalyst for the Removal of Nickel and Cadmium Cations in Batch Experiment

Amal J. M. Al-Hamadani [1]*, Hayder Akram Al-Naseri [1], Ahmed A. Al-Mamoori [2], Nalan Turkoz Karakullukcu [3]

[1] Department of Chemical Engineering, College of Engineering, Tikrit University, Tikrit, Iraq.
[2] Department of Chemical Engineering, College of Engineering, Al-Nahrain University, Baghdad- 10072, Iraq.
[3] Karadeniz Advanced Technology Research and Application Center, Ondokuz Mayis University, Atakum, 55200 Samsun, Turkiye.

Emails:
Amal J. M. Al-Hamadani: amal.j.mohammed42135@st.tu.edu.iq, Hayder Akram Al-Naseri: h.alnasri@tu.edu.iq,
Ahmed A. Al-Mamoori: almamory85@nahrainuniv.edu.iq, Nalan Turkoz Karakullukcu: nturkoz@omu.edu.tr

Abstract:

Wastewater is a critical global issue that must be addressed properly. Photocatalysis is a new technique that integrates approaches to wastewater treatment, particularly cation-based treatment. Herein, ZSM-5 zeolite was used as a photocatalyst to remove Ni and Cd cations from a wastewater stream under ultraviolet (UV) light. The physicochemical features of the ZSM-5-based photocatalyst were investigated using BET surface area, pore volume, XRD, SEM, FTIR, and TGA analyses. Furthermore, different factors were explored, such as the initial cation concentration, ZSM-5 loading, and contact time, to check their influence on the removal of cations' efficiency. It was postulated that the lower the cation concentration, the higher the removal efficiency and the faster the kinetics. For instance, at 12 min and a concentration of 50 ppm, the removal percentages were 99.549% for Ni and 92.282% for Cd. However, the removal percentage decreases for nickel to 47.836% and for Cd to 35.189% at 200 ppm. Moreover, the removal kinetics of cations were also tested under pseudo-first-order and pseudo-second-order models. The pseudo-second-order model fits better than the pseudo-first-order model for both Ni and Cd cations. This study identified a promising photocatalyst for removing metal cations in wastewater treatment.

Keywords:

Cadmium; Heavy metals; Kinetics; Nickel; Cadmium; ZSM-5 Photocatalyst.

Highlights:

- The removal of Nickel and Cadmium cations from wastewater using ZSM-5 was successfully conducted.
- Significant effect for the initial concentration of metals, time reaction, and ZSM-5 dose on the removal efficiency.
- Higher removal efficiency for Nickel and Cadmium was achieved at 99.549% and 92.282%, respectively, at an initial concentration of 50 ppm.
- The pseudo-second-order model fits for both Ni and Cd cations.

Citation:

Al-Hamadani AJM, Al-Naseri H, Al-Mamoori AA, Karakullukcu NT. **Use of ZSM-5 Photocatalyst for the Removal of Nickel and Cadmium Cations in Batch Experiment**. *Tikrit Journal of Engineering Sciences* 2026; **33**(1): 2484.

Article History:

Received:	01	Feb.	2025
Received in revised form:	16	Mar.	2025
Accepted:	06	Apr.	2025
Final Proofreading:	09	Sep.	2025
Available online:	19	May	2026

https://doi.org/10.25130/tjes.33.1.28

Corresponding Author*:

Amal J. M. Al-Hamadani
Department of Chemical Engineering, College of Engineering, Tikrit University, Tikrit, Iraq.
Email: amal.j.mohammed42135@st.tu.edu.iq

1.INTRODUCTION

Heavy metals constitute significant environmental contaminants, especially in aquatic and terrestrial ecosystems. Heavy metal contamination threatens the ecosystem and can adversely affect human health through the food chain. Therefore, it is crucial to identify appropriate strategies for remediating heavy metal pollution. Heavy metals in wastewater can adversely affect all life forms when released directly into the environment [1-4]. Heavy metals in aquatic systems will impede several beneficial uses of water due to rising industrialization. Overexposure to heavy metals like nickel and cadmium can have detrimental effects on human physiology and other biological systems. Environmental concerns about heavy metal contamination are further heightened by the toxicity and permanence of metals in the environment [5]. Typical hazardous contaminants in industrial effluents include heavy metals such as Ni (II) and Cd (II). These metals can be harmful to living things, including people, even at low levels [6]. Various methods have been investigated to mitigate heavy metal contamination, including adsorption, precipitation, filtration, osmosis, and electrolysis [7-9]. Recently, advanced oxidation processes, e.g., photocatalysis, and other advanced techniques have attracted much attention from researchers [10, 11]. A wide range of catalysts, such as TiO_2, WO_3, ZnO, and SnO_2, have been tested for the photodegradation of water contaminants [12]. One chemical process in high demand is photocatalysis, owing to its ease of use, affordability, non-toxicity, high degradation efficiency, and superior stability. UV radiation causes oxidation during the photocatalysis process, and photocatalysts like TiO_2, ZnO, and others sensitize the process [13]. Also, [14], a highly hydrophilic bamboo fiber (BF) membrane with a minimally oxidized Ti_3C_2 (mo-Ti_3C_2) photocatalyst, was developed to create an effective synergistic photocatalytic-photothermal system. To remove heavy metal ions from simulated wastewater, the mo-Ti_3C_2@BF membrane was used. The species, concentration, and light-absorbing and water-transporting structures of heavy metal ions are all methodically tuned. In another investigation [15], an aqueous solution of Syzygium cumin leaf extract was used as a capping agent to create titanium dioxide nanoparticles (TiO_2 NPs). The ability of these environmentally friendly TiO_2 NPs to remove lead from industrial effluent by photocatalysis was further assessed. The authors proposed [16] the effectiveness of Aspergillus niger metabolites as a biocatalyst for the biological synthesis of MgO-NPs. Furthermore, actual textile wastewater and tannery effluents are decolored and degraded using biosynthesized MgO-NPs. Also, the reusability of treated effluents and adsorbents in plant irrigation was examined. Moreover, the ability of biosynthesized MgO-NPs to inhibit harmful bacterial and fungal species was evaluated [17]. A thorough summary of the developments of the photocatalytic method for the treatment of highly contaminated industrial wastewater was reported in the literature. Compared with other wastewater treatment methods, TiO_2-based havephotocatalysts they proven quite effective at breaking down organic pollutants in wastewater. The mechanism of the photocatalyst is significantly influenced by the electrical structure of a semiconductor. The synthesis process, chemical composition, and technical properties all influence a photocatalyst's shape. Reducing the impact of organic contaminants in wastewater will be greatly aided by the photoreactors' increased size. The properties of metal oxides were also reported [18], along with a synopsis of their numerous uses. It focuses on the most prevalent metal oxides—TiO_2, ZnO, WO_3, CuO, and Cu_2O—which are recognised as economical, stable, effective, and, most importantly, ecologically benign for long-term environmental restoration. The photocatalytic activities of these metal oxides, as well as current advancements, difficulties, and adjustments made to these metal oxides to get around their drawbacks and optimize their performance in the photodegradation of pollutants, are highlighted in this paper. Zeolite is an alternative catalyst for photocatalysis in water treatment. Due to the high catalytic activity, shape selectivity, thermal stability, resistance to coke formation, and long catalyst life. Zeolite is an alumina silicate crystal with a three-dimensional framework structure formed by tetrahedral silicate $[SiO_4]^{4-}$ and octahedral alumina $[AlO_4]^{5-}$ that is bundled by an oxygen atom. Each silicon atom is surrounded by 4 oxygen atoms, forming the zeolite network in a regular pattern. In some spots in these networks, the silicon atom is substituted by aluminium, having a coordination number of only 3 oxygen atoms. The existence of aluminium atoms causes the zeolite to have a negative charge that can be used as an ion exchange site with heavy metals, as well as the porous structure of the zeolite that makes it attractive for heavy metals. Zeolite exhibits important characteristics, such as ion adsorption, molecular sieving, and catalytic activity, which show high selectivity in the [19]. Many materials, including metal oxides and mixed metal oxides, are capable of serving as adsorbent materials for different contaminated effluents when formulated and activated correctly [20-23]. ZSM-5 zeolite with the MFI framework has a 3-dimensional channel and a micropore size of 5.1-5.5 Å. Nowadays, ZSM-5

is commonly used as a catalyst and is also used in dewaxing reactions, methanol conversion to gasoline, methanol-to-olefin, hydrocracking, benzene alkylation, NOx reduction, and methane partial oxidation [24]. ZSM-5 zeolite is a promising adsorbent material that can be developed and employed for heavy metal adsorption. In addition, ZSM-5 zeolite has a micropore structure similar to the size of heavy metal ions Ni and Cd. Only a few pieces of information explained the utilization of ZSM-5 zeolite as a heavy metal absorbent. The feasibility of oxidation and reduction reactions depends on the redox potential relative to the semiconductor's CB and VB levels. The photocatalytic reduction of Cd^{2+} and Ni^{2+} can be described by the following mechanisms, as reported by [25, 26]. The mechanism of Ni could go through the way of Eqs. (1) - (4) or Eqs. (5) – (8). However, the Cd reaction mechanism could go to the other route Eq's (5) – (8) based on the literature [25, 26].

- The first step: the UV light hits the semiconductor catalyst, producing electron-hole pairs Eq. (1).
- The second step: The metal ions can be reduced to produce the zero-valence ion Eq. (2).
- The third step: Water can be oxidized to produce H+ and oxygen Eq. (3).
- The fourth step: The metal ions can also be reduced to MO ions Eq. (4).

$$2[H-ZSM-5+hv \rightarrow e^- + h^+] \quad (1)$$

$$Ni^{2+} + 2e^- \rightarrow Ni^0 \quad (2)$$

$$H_2O + 2h^+ \rightarrow \frac{1}{2}O_2 + 2H^+ \quad (3)$$

$$Ni^{2+} + H_2O + hv \rightarrow Ni^0 + \frac{1}{2}O_2 + 2H^+ \quad (4)$$

Lin and Rajeshwar reported the formation of nickel deposition on TiO2 using X-ray photoelectron spectroscopy (XPS) after photocatalytic reaction [27] or it could be possible for both Cd and Ni ions through this way [2].

$$H-ZSM-5+hv \rightarrow e^- + h^+ \quad (5)$$

$$2H_2O + 4h^+ \rightarrow O_2 + 4H^+ \quad (6)$$

$$O^- + h^+ \rightarrow HO^{\cdot} \quad (7)$$

$$M^{n+} + e^- \rightarrow M^{(n-1)+} \quad (8)$$

The objectives of this research are to utilize UV photocatalysis to remove nickel and cadmium metals using the industrial zeolite ZSM-5, study its characterization, and investigate its removal efficiency and selectivity for Ni and Cd heavy metals. To the best of our knowledge, ZSM-5 as a photocatalyst has never been utilized for the removal of nickel and cadmium cation metals from wastewater streams.

2.EXPERIMENTAL WORK

2.1.Preparation of Nickel and Cadmium Solution

A quantity of 2.63 g of the salt Nickel Sulfate ($NiSO_4$) and 1.85 g of the salt Cadmium Sulfate ($CdSO_4$) both materials were obtained from Sigma Aldrich (The USA and Canada), was measured and dissolved in 1000 ml of deionized water in a conical flask both nickel and cadmium prepared separately, resulting in a solution with a concentration of 1000 ppm. The weight of the sample extracted from salt $NiSO_4$ and $CdSO_4$ from Eq. (9).

$$\text{Weight of metal} = \frac{M_{wt} \text{ of salt } \times 1g}{M_{wt} \text{ of metal}} \quad (9)$$

The prepared solutions were stored to prepare other solutions in lighter concentrations.

2.2.Photocatalytic Experimental Procedure

The photocatalytic reactor used was fabricated in-house and was similar to those described by Alvarez and coworkers [28, 29]. It was equipped with eight 6W UVC Phillips G4T5 low-pressure mercury germicidal lamps positioned along the reactor's sidewalls, emitting ultraviolet light at 254 nm to ensure uniform exposure of the slurry to UV radiation. These UV lamps were placed at equal intervals to provide uniform UV irradiation across the reactor and were chosen for their effective output in the germicidal range. The reactor has a stir plate to improve mixing and make it easier for the heavy-metals solution to come into contact with the UV radiation. By keeping the slurry phase suspended, this stirring mechanism enhances the reactor's ability to distribute UV light. A UVP UVX radiometer was used to monitor the spectral irradiance of the UV light source within the reactor. To measure the UV intensity at the point where the heavy metal solution is exposed to light, the radiometer, which has a 254 nm sensor, was set up on the reactor's stir bar. This configuration enables tracking of UV irradiation throughout the experiment to ensure constant exposure and assess its effect on the breakdown of heavy metals, as depicted in Fig. 1. In a typical experiment, 0.5 g of the photocatalyst ZSM-5 zeolite (SiO2/Al2O3) (Thermo Scientific Company, China) was placed in a 100 ml solution containing heavy metals. Different initial concentrations of heavy metals were used, ranging from 50 to 200 ppm. The concentration of the heavy metals in the solution was determined before and after contact with the ZSM-5 zeolite. The experiments were conducted in a photocatalyst reactor under UV irradiation, and 100 ppm of the solution was placed in a beaker on a magnetic stirrer at 400 rpm. The samples were taken (at different time intervals from zero until 40 minutes) by withdrawing samples from the solution using a needle and then filtering the withdrawn solution to get rid of the catalyst residue that may be present in the solution. Then, the heavy metal concentration was analyzed using atomic absorption spectroscopy. Table 1 shows the experiments that were conducted in this investigation.

Table 1 Experimental Runs.

Run	Catalyst	Type of contamination (metal)	Concentration of contaminated/metal (ppm)	Weight of catalyst g/100 mL	Time of reaction (min)	Temperature (°C)
1.	ZSM-5	Ni	50	0.5	40	25
2.	ZSM-5	Ni	100	0.5	40	25
3.	ZSM-5	Ni	150	0.5	40	25
4.	ZSM-5	Ni	200	0.5	40	25
5.	ZSM-5	Cd	50	0.5	40	25
6.	ZSM-5	Cd	100	0.5	40	25
7.	ZSM-5	Cd	150	0.5	40	25
8.	ZSM-5	Cd	200	0.5	40	25
9.	ZSM-5	Ni	100	1.0	40	25
10.	ZSM-5	Ni	100	1.5	40	25

The percentage removal of Ni and Cd was calculated using Eq. (2).

$$\text{Removal percentage} = \frac{(C_o - C_e)}{C_o} \times 100 \quad (10)$$

Where:
C_o: initial metals concentrations (mg/L)
C_e: equilibrium metal concentrations (mg/L)
Meanwhile, the adsorption capacity (q_e, mg/g) at equilibrium was calculated using Eq. (11).

$$q_e = (C_o - C_e) \times \frac{V}{w} \quad (11)$$

Where:
q_e: adsorption capacity (mg/g)
V: volume of the water solution (L)
w: weight of adsorbent (gram).

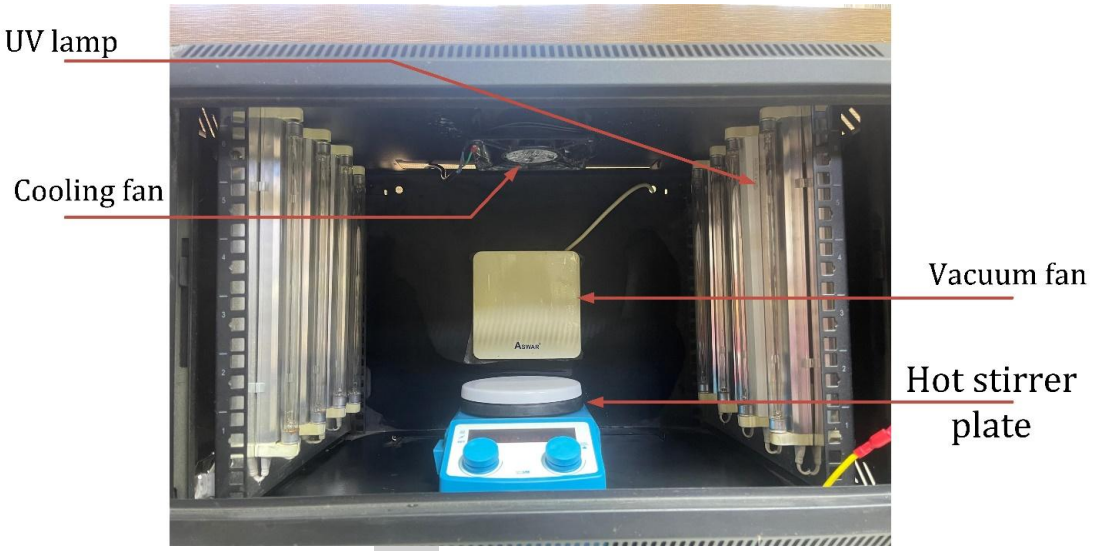

Fig.1 Photocatalytic Reactor.

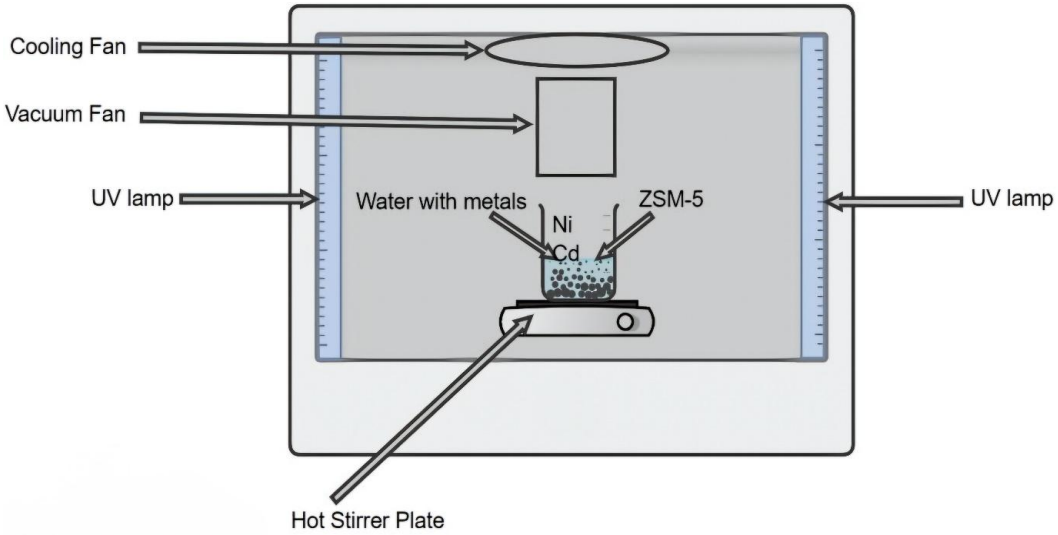

Fig.2 Schematic Diagram of UV Reactor.

3.RESULTS AND DISCUSSION

The removal behavior of Ni and Cd metal ions using zeolite (ZSM-5) has been determined at different concentrations, zeolite doses, and time contacts. The best conditions were observed, and our results showed that the removal process of heavy metal ions by the different natural materials was affected by various parameters such as sorbent dose, contact time, and initial concentration of heavy metal solution.

3.1.Characterization of ZSM-5 Zeolite

The commercial ZSM-5 zeolite was used as it is without further treatment. The performed characterizations of the ZSM-5 material are BET, XRD, SEM, FTIR, and TGA.

3.1.1.Surface Area and Pore Volume

The texture of the ZSM-5 material was determined by employing nitrogen physisorption. This method was used to determine specific surface area, pore volume, and pore size distribution. Bruenne Emmett Teller (BET) method and Barret Joyner Halenda (BJH) were used to determine the specific surface area and pore volume of the ZSM-5 zeolite, respectively. The result showed that the bare ZSM-5 zeolite has a surface area of 288.88 m^2/g, pore volume of 0.151 cm^3 /g, and pore radius Dv(r) 1.888 nm [19]. The BET results after the reaction showed that the surface area of ZSM-5 when removing nickel metal is 268.0532 m^2/g. In comparison, the surface area after removing cadmium metal was 232.7521 m2/g, indicating a decrease in the surface area of ZSM-5 after the removal of heavy metals. This decrease is related to several factors, including the adsorption of metal ions. The initial interaction of Ni and Cd ions with ZSM-5 may lead to metal ion adsorption on the ZSM-5 zeolite surface. The process may temporarily enhance the catalyst's active-site availability. The metal ions being adsorbed can occupy the pores and channels of the structure, thereby blocking them. This blockage can reduce the effective surface area available for further reaction and adsorption. Structural alterations in the ZSM-5 framework may result from high concentrations of nickel and cadmium. If the zeolite structure incorporates ions, they may alter the stability and integrity of the framework, which could reduce surface area. It is plausible that during the photocatalytic process with ZSM-5, leaching may occur, especially when the metal interacts with the zeolite. Figure 2 shows the adsorption isotherm of the ZSM-5 zeolite material. As depicted in Fig. 2, the ZSM-5 material follows type I and type IV shapes, which correspond to the microporous and mesoporous materials. These findings are consistent with the IUPAC classification of the zeolite material. The high curvature in the amount adsorbed at low P/Po supports the presence of small pores (micropores), which are rapidly filled by adsorbate (gas) molecules. The gradual rise in higher relative pressures also confirms the presence of some mesopores or macropores in the material [30]. The existence of a hysteresis loop (type H4), however, affirms the characteristics of the mesoporous zeolite materials.

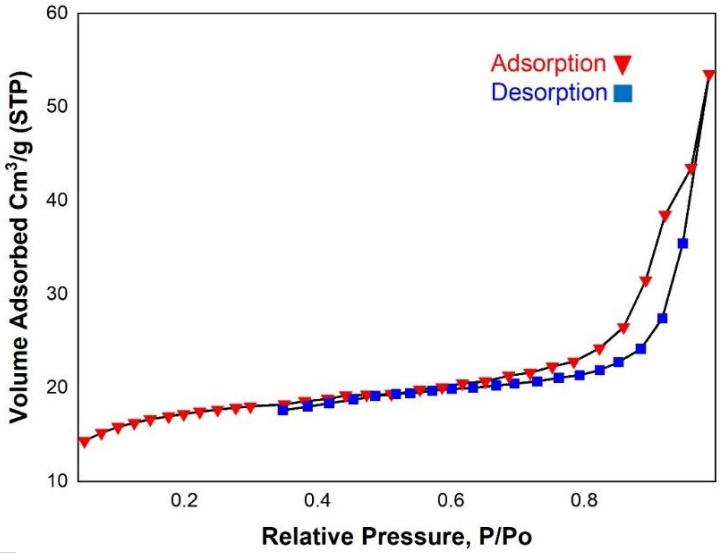

Fig. 3 Adsorption and Desorption Isotherm of ZSM-5 Synthetic Zeolite.

3.1.2.Powder X-Ray Diffraction (XRD)

X-ray diffraction (XRD) was utilized to analyze the crystallinity of the ZSM-5 material structure, as illustrated in Fig. 3. The XRD pattern of the ZSM-5 materials was performed before and after subjecting the materials to the Ni and Cd metal ions. All ZSM-5 samples exhibited the same diffraction peaks. The peaks of the ZSM-5 zeolite are positioned at the following angles (2θ) 7.858°, 22.996°, 23.224°, and 23.810°, which are related to the typical ZSM-5 structure [31-33]. These findings indicate that the XRD patterns of the ZSM-5 catalyst materials before and after exposure to

heavy metals show a well-defined crystalline structure, as evidenced by sharp, distinct diffraction peaks. The XRD findings clearly show that the membrane has enough crystallinity and that the concentration of the zeolite component can be used to adjust the membrane's crystallinity [34]. It can be noticed that the intensity of the characteristic peaks of the bare ZSM-5 material is similar to that of ZSM-5 after being subjected to cadmium and nickel, indicating that the crystallinity of the ZSM-5 material is retained even after using photocatalytic.

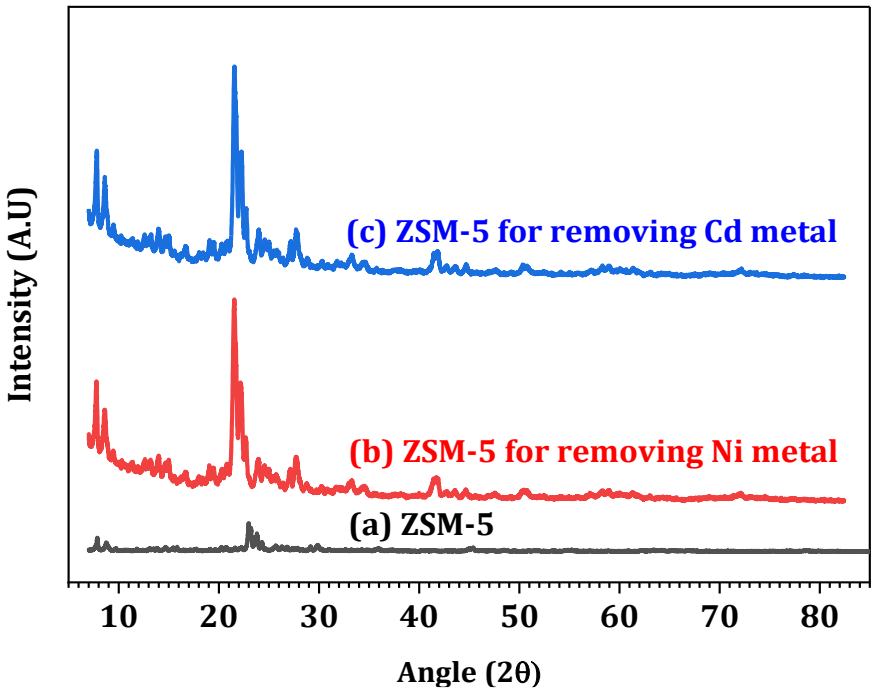

Fig. 4 XRD Patterns of ZSM-5 Synthetic Zeolite (a) ZSM-5 (b) ZSM-5 after Subjecting to Ni Ions (c) ZSM-5 after Subjecting to Cd Ions.

3.1.3.Scanning Electron Microscopy (SEM)

Scanning electron microscopy (SEM) was performed to evaluate the crystallite size and morphology of the catalysts used [35]. The morphology of ZSM-5 has a hexahedral structure, in agreement with the ZSM-5 characteristics from a previously reported study [36]. The morphology of the bare ZSM-5, ZSM-5 after subjecting to Ni ions, and ZSM-5 after subjecting to Cd ions was illustrated in Fig. 4. Figure 4 (a) reveals aggregated clusters of small, crystalline particles of the bare ZSM-5. The ZSM-5 material typically forms faceted, blocky crystals due to its well-ordered crystalline structure, as evidenced in the image [33]. These crystals appear as angular, plate-like, or prismatic structures, which is consistent with the morphology of ZSM-5. The sharp edges and well-defined shapes indicate a high degree of crystallinity, which is typical for pure ZSM-5. The uniformity in shape and size of these crystalline particles suggests good crystallinity, meaning that the ZSM-5 sample was synthesized under optimal conditions. The well-formed crystal shapes are indicative of an ordered, stable structure [19]. High crystallinity is advantageous in applications such as catalysis and adsorption as it ensures a consistent pore structure throughout the material, allowing predictable performance. The presence of mesoporous interparticle spaces, with inherent microporosity (not visible in SEM), critical for catalytic and adsorption applications and the internal microporous framework of ZSM-5 (with pores ~5.5 Å in diameter) is essential for its catalytic and adsorption properties. The image scale (1 µm bar) shows that the individual ZSM-5 crystals are submicron to micrometer-sized. These particles appear to form larger aggregates, which may affect how the material packs and the accessibility of the micropores for adsorption or catalysis. Smaller particle sizes and aggregates with interconnected pores provide additional pathways for molecular diffusion, increasing the efficiency of ZSM-5 in applications requiring high surface area. Ideal for catalysis, adsorption, and ion exchange due to its high surface area, porosity, and stable structure. This SEM image confirms that the ZSM-5 sample is well-suited for applications requiring high surface area and crystalline stability. The morphology aligns with expectations for pure ZSM-5 and suggests good synthesis quality, resulting in a material optimized for catalysis and adsorption purposes. Figure 4 (b,c) ZSM-5's micro- and mesoporous structure provides numerous adsorption sites for capturing heavy metal ions. The pores and rough texture allow metal ions like Ni and Cd to diffuse into the structure and

adsorb onto active sites within the channels. The porous nature of the structure, as shown by SEM, suggests that there are sufficient pathways for these metal ions to enter the ZSM-5 framework, thereby enhancing the material's efficiency in removing contaminants from solutions. ZSM-5 is efficient for heavy metal adsorption due to its porous structure and ion-exchange capability, and it has potential for reuse. This made it feasible to verify that during the ion exchange treatments, the particle sizes and morphologies remained constant [35]. This SEM image confirms that the ZSM-5 catalyst has the necessary morphology, surface area, and crystallinity to function effectively as an adsorbent for Ni and Cd ions. Its porous structure is well-suited for capturing and immobilizing heavy metal ions, making it an excellent choice for environmental remediation applications.

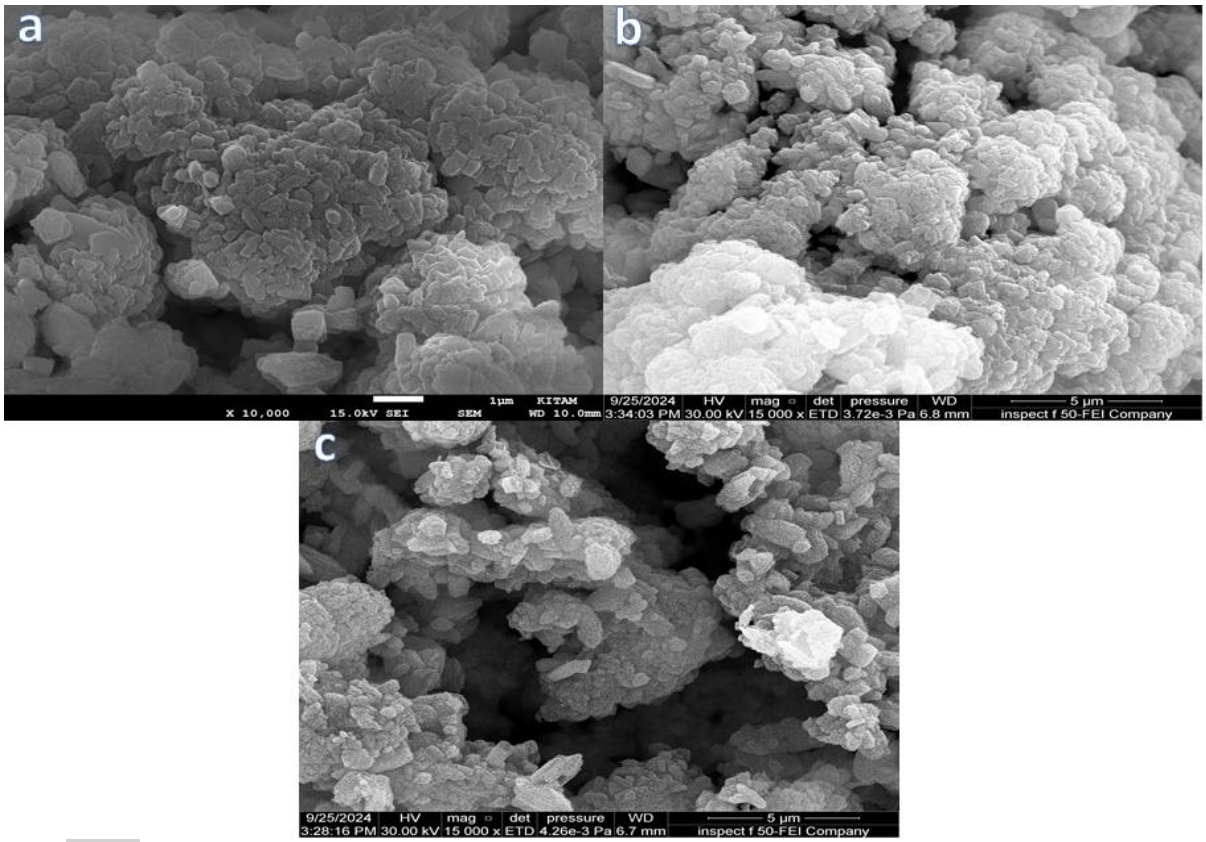

Fig. 5 SEM (a) ZSM-5 (b) ZSM-5 for Removing Ni Metal (c) ZSM-5 for Removing Cd Metal.

3.1.4.Fourier Transform Infrared (FTIR)

Fourier Transform Infrared Spectroscopy (FT-IR) is an analytical method employed to determine the molecular makeup of a given sample. FT-IR can discern the chemical compounds present in a sample by analyzing the wavelengths that are absorbed when infrared light is incident upon the sample. It finds extensive application in chemistry, materials science, and pharmaceutical research. The spectral range of the samples was 500–4000 cm-1. The variation in dipole moment is directly proportional to the amplitude of the FT-IR band. As a result, compounds characterized by polar bonds, such as OH, display a conspicuous infrared band, while those employing covalent bonds, like N=N, manifest a band of lesser prominence. Vibrational frequencies (v) tend to increase in magnitude as the mass of the vibrating elements decreases, and the bonds become more robust. Figure 5 illustrates the FT-IR characteristics of the ZSM-5. The peak at 3636 cm^{-1} is attributed to the stretching frequency of isolated silanol groups, Si–O–H bond, while the peak at 1649 cm^{-1} is attributed to adsorbed water [37, 38]. Absorption bands at 453 cm^{-1} (T–O bending), 793 cm^{-1} (external symmetric stretching), 1078 cm^{-1} (internal asymmetric stretching), and 1227 cm^{-1} (external asymmetric stretching) correspond to siliceous materials [39, 40]. In general, comparing the FT-IR spectrum of the sample containing cadmium and nickel metals with the pure zeolite spectrum, we can conclude that there is a small decrease in the peak's intensity, broadening and shifting of the peak at 549 cm^{-1} to 540 cm-1 and 544 cm^{-1}. This is evidence that zeolite is not much affected by the presence of cadmium pollutants and nickel with photocatalytic activity and does not affect the framework structure of ZSM-5 zeolite, and this reflects that the ZSM-5 zeolite is good for removing heavy metals from water [41].

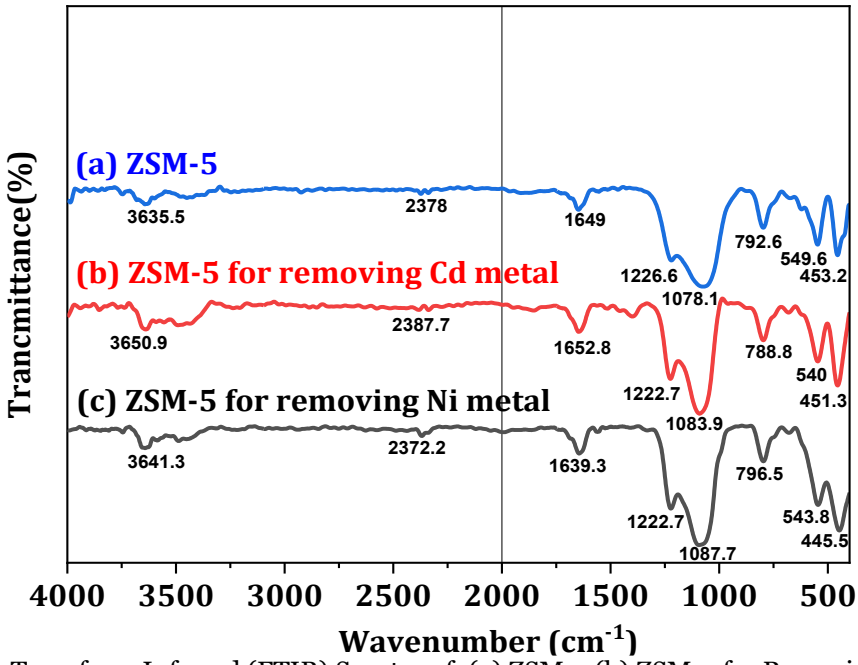

Fig. 6 Fourier Transform Infrared (FTIR) Spectra of; (a) ZSM-5 (b) ZSM-5 for Removing Cd Metal (c) ZSM-5 for Removing Ni Metal.

3.1.5.Thermal Gravimetric Analysis (TGA)

The thermal stability of the bare ZSM-5 was tested as shown in Fig. 6 using thermogravimetric Analysis (TGA). The TGA curve shows a small decline in the weight percentage around (94%) at temperatures below 200 °C, which could be related to moisture and atmospheric gases adsorbed by the ZSM-5 material [32, 42, 43]. The first step of weight loss, which is associated with the desorption of water molecules, was observed to occur between 25 and 350°C. Stronger water molecules are lost over time, whereas weakly bound ones are lost instantly. The second stage, which was shown to occur between 350 and 500°C, is associated with weight loss due to the template's thermal lysis [44]. The water loss increased as the Si/Al ratio dropped. It may be explained by the fact that the zeolite with the highest silicon content has less water, since it is more hydrophilic due to its higher acidity at lower Si/Al ratios [45, 46]. The removal of physically attached water molecules from the sample's surface caused an initial weight reduction in the TGA of the ZSM-5 catalyst, both unmodified and modified, at 100 °C [47]. Gradual weight loss between 200°C and 800°C, suggesting the removal or decomposition of certain components within the ZSM-5 catalyst [48]. The weight stabilizes at around 90% at temperatures above 800°C, indicating that the catalyst material is relatively stable at higher temperatures.

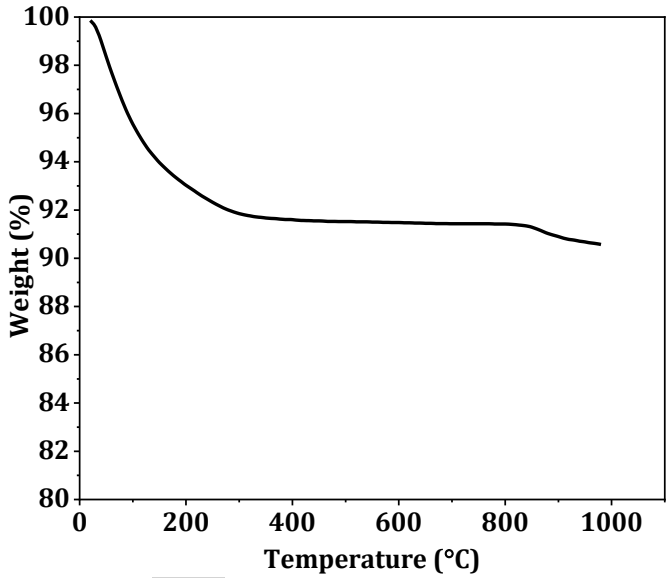

Fig. 7 TGA for Zeolite (ZSM-5).

3.2.1.Effect of the Initial Concentration

The effect of the initial concentration on the retention of metal ions, at concentration levels ranging from 50 to 200ppm (mg/L) is shown in Fig. 7. Batch experiments were carried out with a constant agitation speed and at ambient temperature. The figure shows that the removal percentage of the heavy metal ions at different concentrations first increases at 12 min. At a concentration of 50 ppm, the removal percentage for Ni was 99.549%, and for Cd was 92.282%. The removal percentage decreases with increasing pollutant concentration: 47.836% for nickel and 35.189% for Cd at 200 ppm. This is due to the increase in the percentage of the pollutant, as when the concentration of the pollutant increases, all the pores on the surface of the catalyst are occupied, which requires a longer time to achieve complete removal [49]. Increasing the initial concentration of Ni(II) can effectively enhance the limitation of mass transfer between the solid and aqueous phases, resulting in increased metal ion adsorption [50].

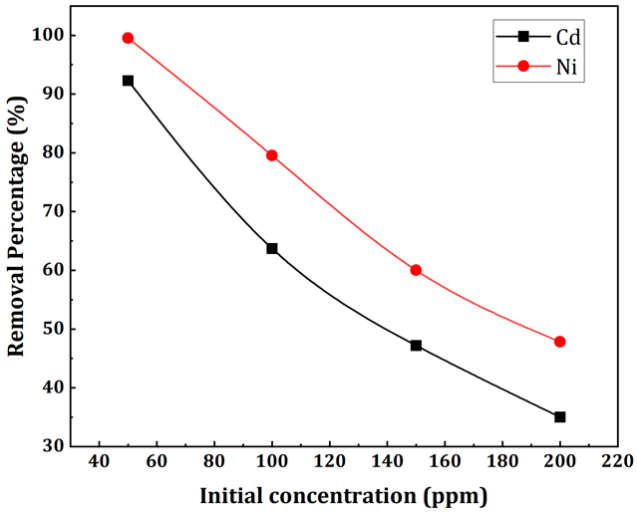

Fig. 8 Effect of Initial Nickel Concentrations for Removal Percentage by ZSM-5.

3.2.2.The Effect of the ZSM-5 Loading

The effect of the removal percentage of metal ions on the ZSM-5 zeolite loading was studied at different loading ranges from 0.5 to 1.5 g in a constant volume solution of 100 ml and a pollutant concentration of 100 ppm with a stirring time of 40 min. As is clear from Fig. 8, the results indicated that the removal percentage increased considerably with the increasing dose of the sorbent for nickel [51]. With an increase in sorbent weight, there are more binding sites available to remove metal ions at a given starting metal ion concentration [50]. A significant amount of adsorbent effectively reduces the degree of unsaturation of the adsorbent sites, hence lowering the number of such sites per unit mass. This might be caused by two factors. Less Ni (II) is adsorbed as a result, and (ii) particles overlap in the beads because of the high adsorbent content, which lowers the total surface area and lengthens the diffusion route. Removal per unit mass decreased as a result of these two causes [52].

3.2.3.The Effect of Contact Time

The percentage of heavy metal removal increased with time at different initial pollutant concentrations. Figure 9 shows that the removal efficiency of the Ni ions reached equilibrium (99.195%) after 10 min at a concentration of 50 ppm with sharp kinetic behavior, while for other concentrations, the removal efficiency increases gradually with time. It was observed that the removal rate at a concentration of 100 ppm after 20 minutes reached 90.989%, while for a concentration of 150 ppm, it reached 90.345%, and for 200 ppm, it reached 53.14%. This gradation in the removal rate is due to the change in the concentration of the pollutant, as the lower the concentration of the pollutant, the faster it is removed due to the presence of vacant sites on the surface of the catalyst that carry out the reaction process in lower time [53]. However, at high concentrations, it takes longer to complete the reaction and empty the sites on the catalyst's surface, replacing them with other pollutant molecules. Figure 10 shows that the removal efficiency of Cd ions reached equilibrium (98.5856%) after 10 min at 50 ppm, whereas at 100 ppm and 150 ppm, it reached equilibrium at 72.1958% and 65.2147% after 20 min. At a cadmium concentration of 200 ppm, the removal rate increases gradually over time and reaches 67.6292% after 30 min, which is higher than the cadmium removal rate at 150 ppm. The instability in the removal rate at 200 ppm is due to the high percentage of pollutants, as the pollutant molecules attack the catalyst surface and occupy it continuously over time, causing instability at the beginning of the reaction, which requires a longer time for the removal process to be fully completed. As a result, the adsorption rate slows down during the later period.

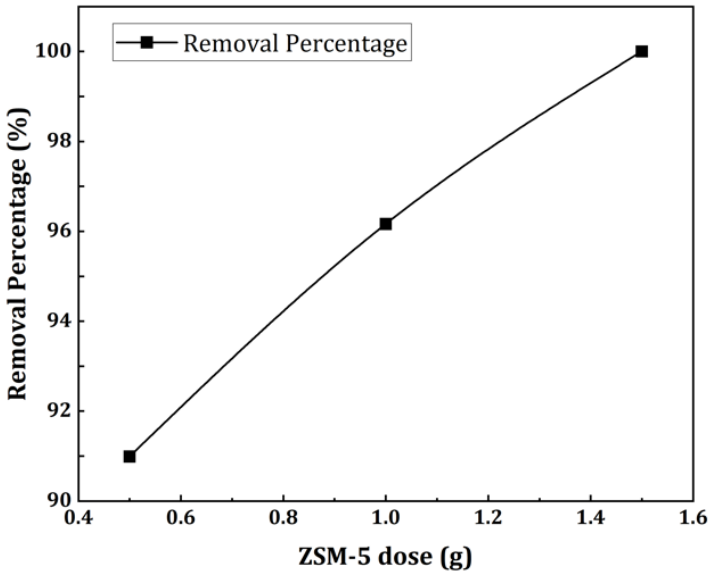

Fig. 9 Effect of Zeolite Dose on the Removal of Heavy Metal Ions.

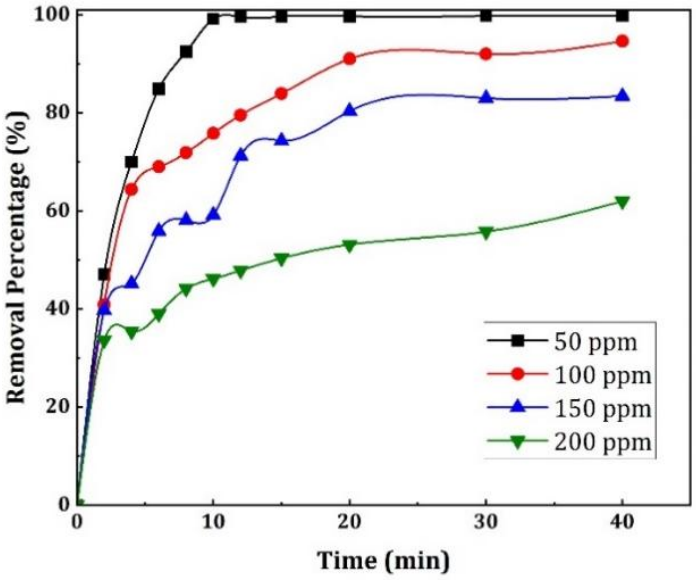

Fig. 10 Effect of Contact Time for Nickel Concentration for Removal Percentage by ZSM-5.

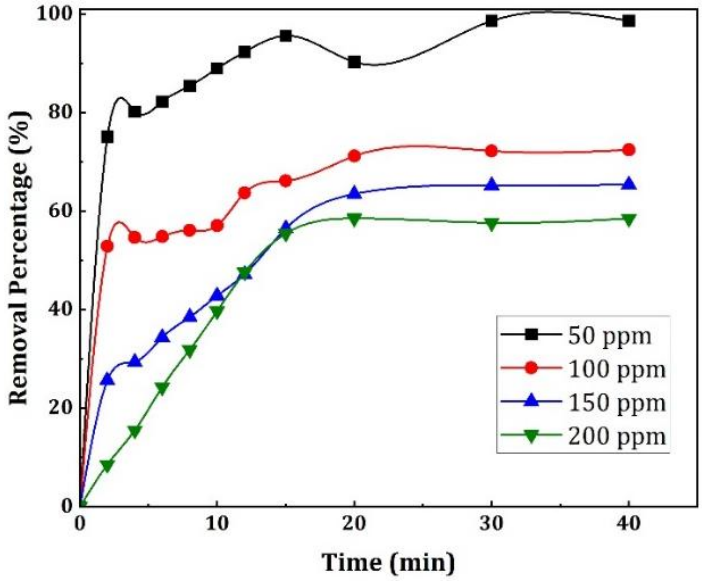

Fig. 11 Effect of Contact Time for Cadmium Concentrations for Removal Percentage by ZSM-5.

3.2.4.Kinetic Reaction Models

The kinetics of Nickel and Cadmium removal by ZSM-5 was analyzed by pseudo-first-order and pseudo-second-order models as shown in Eq. (12) and (13). The agreement between the models' predicted values and experimental data was quantified using the coefficient of determination (R^2). The model with a relatively high coefficient of determination fits better for describing the removal kinetics.

$$\ln\left(\frac{C_o}{C_t}\right) = k_1 t \qquad (12)$$

$$\frac{1}{C_t} - \frac{1}{C_o} = k_2 t \qquad (13)$$

where:

C_o= initial concentration mg/L

C_t= concentration at the time of sampling mg/L

k_1= rate constants of pseudo-first-order (min^{-1})

k_2= rate constants of pseudo-second-order ($L\ mg^{-1}min^{-1}$)

Figures 11 and 12 show plots of ln (C_o/C_t) and $1/C_t$ versus irradiation time, which represent the pseudo-first-order and pseudo-second-order models, respectively. As shown in these figures, the experimental results demonstrate a linear degradation fit for Ni and Cd. From the results shown in Figs. 11 and 12 revealed that models considered, the pseudo-second-order kinetic equation provided higher R^2 values, thus, the removal of Ni and Cd ions from aqueous solutions by ZSM-5 were found to appropriately follow the pseudo-second-order kinetic equation. shows the second-order rate constant (k_2) (obtained from kinetic plots of Fig. 12 and corresponding determination coefficients (R^2) values for the removal of Ni and Cd using a UV light source with photocatalysts. These findings showed that, of the two models examined, the pseudo-second-order kinetic equation produced higher R^2 values; hence, it was determined that the removal of Ni(II) ions from aqueous solutions by SDS-ZSM-5 followed the pseudo-second-order kinetic equation [54, 55].

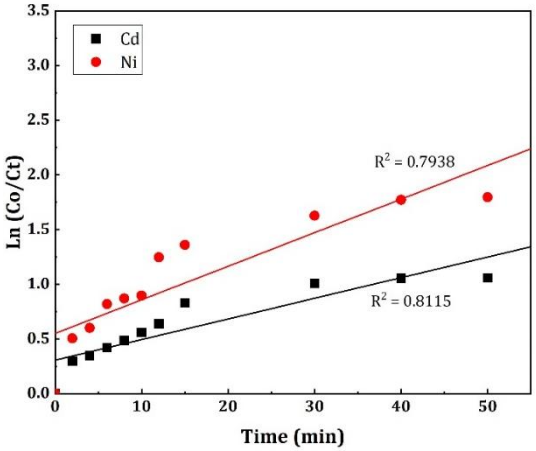

Fig. 12 The Plot of Ln (Co/Ct) Versus Irradiation Time Follows Pseudo-First-Order Kinetics for the Removal of Nickel and Cadmium by Photocatalysts under UV Light.

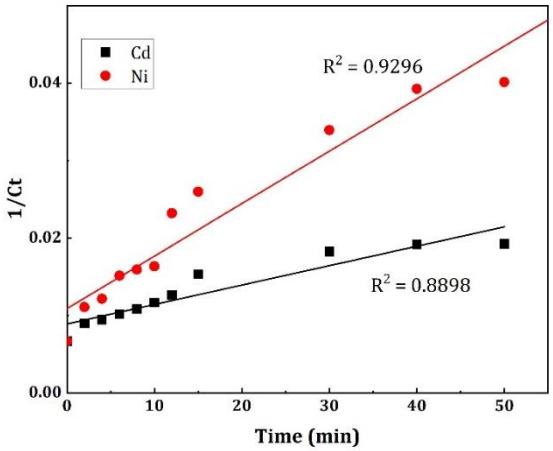

Fig. 13 The plot of 1/Ct Versus Irradiation Time Follows Pseudo-Second-Order Kinetics for the Removal of Nickel and Cadmium by Photocatalysts under UV Light.

Table 2 Pseudo-First Order, Pseudo-Second Order, and Values of k and R^2.

Metal Ion	Pseudo-First Order		Pseudo-Second Order	
	k_1 (min^{-1})	R^2	k_2($L\ mg^{-1}min^{-1}$)	R^2
Nickel	0.052	0.7938	0.002	0.9296
Cadmium	0.018	0.8115	0.0003	0.8898

4.CONCLUSIONS

The utilization of ZSM-5 photocatalyst in wastewater treatment has attracted much attention from researchers. In this study, ZSM-5 zeolite was employed as a photocatalyst to treat Ni and Cd cations from the wastewater stream. The initial cation concentration, ZSM-5 loading, and contact time were investigated to study their impact on the removal cations' efficiency. It was found that at low cation concentrations, the catalyst achieved higher removal efficiency and faster kinetics. For example, at 12 min with a concentration of 50 ppm, the removal percentages were 99.549% for Ni and 92.282% for Cd. On the other hand, the removal percentage of the heavy metals drops to 47.836% for nickel and 35.189% for Cd at 200 ppm. In the meantime, a kinetic study was also performed employing pseudo-first-order and pseudo-second-order models. The pseudo-second-order model fits better than the pseudo-first-order model for both Ni and Cd cations. The proposed ZSM-5 catalyst mechanism for both Ni and Cd cations was considered in terms of electron-hole creation, with a different route for each cation. Lastly, physicochemical analyses such as BET, XRD, SEM, and FTIR were performed for the fresh and the used ZSM-5 photocatalysts.

NOMENCLATURE

BET	Bruenne Emmett Teller
XRD	X-ray diffraction
SEM	Scanning electron microscopy
TGA	Thermal gravimetric analysis
FTIR	Fourier Transform Infrared Spectroscopy
C_o	initial concentration mg/L
C_e	equilibrium metals concentrations (mg/L)
C_t	concentration at the time of sampling mg/L
q_e	adsorption capacity (mg/g)
k_1	rate constants of pseudo-first-order (min^{-1})
k_2	rate constants of pseudo-second-order ($L\ mg^{-1}min^{-1}$)

REFERENCES

[1] Heidari A, Younesi H, Mehraban Z. **Removal of Ni (II), Cd (II), and Pb (II) from a Ternary Aqueous Solution by Amino Functionalized Mesoporous and Nano Mesoporous Silica.** *Chemical Engineering Journal* 2009; **153**(1-3): 70-79.

[2] Chen YH, Li FA. **Kinetic Study on Removal of Copper (II) Using Goethite and Hematite Nano-Photocatalysts.** *Journal of Colloid and Interface Science* 2010; **347**(2): 277-281.

[3] Mahdy SA, Al-Naseri H. **Effect of Magnesium Oxide Nanoparticles (MgO) on Wastewater Treatment and Electric Current Generation Using Microbial Fuel Cell Technology.** *Tikrit Journal of Engineering Sciences* 2024; **31**(2): 219-228.

[4] Numaan MM, Al-Janabi SAS, Al-Sanjary AAM, Al-Musawi AA. **Study the Possibility of Using the Treated Industrial Wastewater of North Refineries Company, Baiji-Iraq, for Irrigation Purposes.** *Tikrit Journal of Engineering Sciences* 2024; **31**(4): 183-190.

[5] Bahadir T, Bakir G, Sandal S, Genç A. **The Investigation of Lead Removal by Biosorption: An Application at Storage Battery Industry Wastewaters.** *Enzyme and Microbial Technology* 2007; **41**(1-2): 98-102.

[6] Barakat M, Chen Y, Huang C. **Removal of Toxic Cyanide and Cu (II) Ions from Water by Illuminated TiO2 Catalyst.** *Applied Catalysis B: Environmental* 2004; **53**(1): 13-20.

[7] Buasri A, Chaiyut N, Loryuenyong V, Worasan S, Tippakorndaj N. **Use of Natural Clinoptilolite for the Removal of Lead (II) from Wastewater in Batch Experiment.** *Chiang Mai Journal of Science* 2008; **35**(3): 447-456.

[8] Minceva M, Markovska L, Meshko V. **Removal of Zn 2+, Cd 2+ and Pb 2+ from Binary Aqueous Solution by Natural Zeolite and Granulated Activated Carbon.** *Macedonian Journal of Chemistry and Chemical Engineering* 2007; **26**(2): 125-134.

[9] AlRubaye SF, Al Haboubi NA, Al-Amili HA. **Removal of Sulfate and Iron from a Water Solution Using a New Flow Pattern in an Electrocoagulation Reactor.** *Tikrit Journal of Engineering Sciences* 2024; **31**(2): 205-218.

[10] Robinson T, McMullan G, Marchant R, Nigam P. **Remediation of Dyes in Textile Effluent: A Critical Review on Current Treatment Technologies with a Proposed Alternative.** *Bioresource Technology* 2001; **77**(3): 247-255.

[11] Mittal A, Malviya R, Mittal J, Kurup L. **Studies on the Adsorption Kinetics and Isotherms for the Removal and Recovery of Methyl Orange from Wastewaters Using Waste Materials.** *Journal of Hazardous Materials* 2007; **148**(1): 229-240.

[12] Alinsafi A, Khemis M, Pons MN, Leclerc JP, Yaacoubi A, Benhammou A, Nejmeddine A. **Treatment of Textile Industry Wastewater by Supported Photocatalysis.** *Dyes and Pigments* 2007; **74**(2): 439-445.

[13] Nakata K, Fujishima A. **TiO2 Photocatalysis: Design and Applications.** *Journal of Photochemistry and Photobiology C: Photochemistry Reviews* 2012; **13**(3): 169-189.

[14] Wang F, Wang Z, Zhao S, Zhang S, Tan J, Zhao Y, Zhang L, Qin J, Yuan M. **Removal and Reuse of Heavy Metal Ions on Mildly Oxidized Ti3C2@ BF Membrane via Synergistic Photocatalytic-Photothermal Approach.** *Journal of Hazardous Materials* 2023; **458**: 131954.

[15] Sethy NK, Sharma Z, Kumar A, Sahoo PK, Patra JK. **Green Synthesis of TiO2 Nanoparticles from Syzygium cumini Extract for Photo-Catalytic Removal of Lead (Pb) in Explos Industrial Wastewater.** *Green Processing and Synthesis* 2020; **9**(1): 171-181.

[16] Fouda A, Hassan SE, Saied E, Eid AM, Awad MA, Al-Askar AA, Hashem AH. **Photocatalytic Degradation of Real Textile and Tannery Effluent Using Biosynthesized Magnesium Oxide Nanoparticles (MgO-NPs), Heavy Metal Adsorption, Phytotoxicity, and Antimicrobial Activity.** *Journal of Environmental Chemical Engineering* 2021; **9**(4): 105346.

[17] Al-Nuaim MA, Alwasiti AA, Shnain ZY. **The Photocatalytic Process in the**

Treatment of Polluted Water. *Chemical Papers* 2023; **77**(2): 677-701.

[18] Danish MSS, Bhattacharya A, Stepnov AM, Sabique MK, Zaheb H, Shikh Ali AS, Senjyu T. **Photocatalytic Applications of Metal Oxides for Sustainable Environmental Remediation.** *Metals* 2021; **11**(1): 80.

[19] Mukti RR. **Characteristics of Heavy Metals Adsorption Cu, Pb and Cd Using Synthetics Zeolite Zsm-5.** *Journal of Tropical Soils* 2016; **20**(2): 77-83.

[20] Al-Mamoori A, Al-Jubouri SM, Lawson S, Rownaghi AA, Rezaei F. **Novel Bi-SBA-15 Derived Rice Husk for Iodine Adsorption from Off-Gas Stream.** *Results in Chemistry* 2025; **13**: 101972.

[21] Mohammed MR, Shabeeb HA, Al-Rubaie AA. **Preparation and Diagnosis of Activated Carbon from Hydrothermally Carbonized Sucrose as an Adsorption for the Removal Methyl Red Dye from Aqueous Synthetic Solutions.** *Iranian Journal of Chemistry and Chemical Engineering* 2024; **43**(4).

[22] Hameed MS, Mohammed AA, Al-Mamoori A, Lawson S, Rezaei F, Rownaghi AA. **Assembly of 2D/2D Bi2WO6/Boron-Doped g-C3N4 Z-Type Heterojunction Photocatalysts for Efficient Antibiotic Adsorption and Degradation.** *Materials Science in Semiconductor Processing* 2024; **180**: 108591.

[23] Al-Mamoori A, Lawson S, Rownaghi AA, Rezaei F. **Development of Sodium-Based Borate Adsorbents for CO2 Capture at High Temperatures.** *Industrial & Engineering Chemistry Research* 2023; **62**(8): 3695-3704.

[24] Cejka J, Van Bekkum H. **Zeolite and Ordered Mesoporous Materials: Progress and Prospect Czech Republic.** The 1st FEZA School on Zeolites. Pague Studies in Surface Science and Catalysis; 2005; 157.

[25] Shirzad Siboni M, Samadi MT, Yang JK, Lee SM. **Photocatalytic Removal of Cr (VI) and Ni (II) by UV/TiO2: Kinetic Study.** *Desalination and Water Treatment* 2012; **40**(1-3): 77-83.

[26] Chowdhury P, Elkamel A, Ray AK. **Photocatalytic Processes for the Removal of Toxic Metal Ions.** 2014.

[27] Lin WY, Rajeshwar K. **Photocatalytic Removal of Nickel from Aqueous Solutions Using Ultraviolet-Irradiated TiO2.** *Journal of the Electrochemical Society* 1997; **144**(8): 2751.

[28] Long M, Brame J, Qin F, Bao J, Li Q, Alvarez PJJ. **Phosphate Changes Effect of Humic Acids on TiO2 Photocatalysis: From Inhibition to Mitigation of Electron–Hole Recombination.** *Environmental Science & Technology* 2017; **51**(1): 514-521.

[29] Liu D, Wu J, Zhang G, Wang S, Yuan D, Zhao J. **Perfluorooctanoic Acid Degradation in the Presence of Fe (III) under Natural Sunlight.** *Journal of Hazardous Materials* 2013; **262**: 456-463.

[30] Li H, Zhou J, Zhang G, Ren H, Wang M, Zhou Y, Long Y. **Synthesis and Photocatalytic Activity of Hierarchical Zn-ZSM-5 Structures.** *Catalysts* 2021; **11**(7): 797.

[31] Xin M, Xu S, Dong M, Guo F, Wei J. **Influence of Status of Zn Species in Zn/ZSM-5 on Its Catalytic Performance.** *Petroleum Processing and Petrochemicals* 2019; **50**: 42-50.

[32] Pan Y, Wang G, Gao J, Jiang W, Zhao Z. **Enhanced Photocatalytic Oxidation Degradability for Real Cyanide Wastewater by Designing Photocatalyst GO/TiO2/ZSM-5: Performance and Mechanism Research.** *Chemical Engineering Journal* 2022; **428**: 131257.

[33] Pan Y, Gao J, Wang G, Jiang W, Zhao Z. **Synergistic Effect of Adsorptive Photocatalytic Oxidation and Degradation Mechanism of Cyanides and Cu/Zn Complexes over TiO2/ZSM-5 in Real Wastewater.** *Journal of Hazardous Materials* 2021; **416**: 125802.

[34] Sabarish R, Unnikrishnan G, Shaji S, Nair S. **Fabrication of PVA/Agar/Modified ZSM-5 Zeolite Membrane for Removal of Anionic Dye from Aqueous Solution.** *International Journal of Environmental Science and Technology* 2021; **18**(9): 2571-2586.

[35] Coelho A, Fonseca IM, Lemos MA, Lemos F. **The Effect of ZSM-5 Zeolite Acidity on the Catalytic Degradation of High-Density Polyethylene Using Simultaneous DSC/TG Analysis.** *Applied Catalysis A: General* 2012; **413**: 183-191.

[36] Satriyatama A, Rospitasari A, Prasetyo I, Mukti RR. **ZnO-Incorporated ZSM-5 for Photocatalytic CO2 Reduction into Solar Fuels under UV–Visible Light.** *Chemistry Proceedings* 2021; **6**(1): 1.

[37] Rahmani F, Haghighi M, Mahboob S. **Hydrogen Production via CO2 Reforming of Methane over ZrO2-Doped Ni/ZSM-5 Nanostructured Catalyst Prepared by Ultrasound**

Assisted Sequential Impregnation Method. *Journal of Power Sources* 2014; **272**: 816-827.

[38] Aghamohammadi S, Haghighi M, Karimipour S. **A Comparative Synthesis and Physicochemical Characterizations of Ni/Al2O3–MgO Nanocatalyst via Sequential Impregnation and Sol–Gel Methods Used for CO2 Reforming of Methane.** *Journal of Nanoscience and Nanotechnology* 2013; **13**(7): 4872-4882.

[39] Khatamian M, Divband B, Jodaei A. **Degradation of 4-Nitrophenol (4-NP) Using ZnO Nanoparticles Supported on Zeolites and Modeling of Experimental Results by Artificial Neural Networks.** *Materials Chemistry and Physics* 2012; **134**(1): 31-37.

[40] Sabarish R, Unnikrishnan G. **A Novel Anionic Surfactant as Template for the Development of Hierarchical ZSM-5 Zeolite and Its Catalytic Performance.** *Journal of Porous Materials* 2020; **27**: 691-700.

[41] Haghighi M, Rahmani F, Mazaheri AS. **Photocatalytic Reduction of Cr (VI) in Aqueous Solution over ZnO/HZSM-5 Nanocomposite: Optimization of ZnO Loading and Process Conditions.** *Desalination and Water Treatment* 2017; **58**: 168-180.

[42] Ma Y, Liu Z, Wu W, Jiang Z, Sun JH. **Synthesis, Characterization and Catalytic Activity of a Novel Mesoporous ZSM-5 Zeolite.** *Materials Research Bulletin* 2013; **48**(5): 1881-1884.

[43] Zhang Y, Jin C. **Rapid Crystallization and Morphological Adjustment of Zeolite ZSM-5 in Nonionic Emulsions.** *Journal of Solid State Chemistry* 2011; **184**(1): 1-6.

[44] Frantz TS, Moraga GC, Santos MJ, Rodrigues AE. **Synthesis of ZSM-5 with High Sodium Content for CO2 Adsorption.** *Microporous and Mesoporous Materials* 2016; **222**: 209-217.

[45] Wu G, Liu S, Wang J, Zhang L, Wang X. **Nanosized ZSM-5 Zeolites: Seed-Induced Synthesis and the Relation Between the Physicochemical Properties and the Catalytic Performance in the Alkylation of Naphthalene.** *Microporous and Mesoporous Materials* 2013; **180**: 187-195.

[46] Ali M, Brisdon B, Thomas W. **Synthesis, Characterization and Catalytic Activity of ZSM-5 Zeolites Having Variable Silicon-to-Aluminum Ratios.** *Applied Catalysis A: General* 2003; **252**(1): 149-162.

[47] Sabarish R, Unnikrishnan G. **Synthesis, Characterization and Evaluations of Micro/Mesoporous ZSM-5 Zeolite Using Starch as Bio Template.** *SN Applied Sciences* 2019; **1**: 1-13.

[48] Stankovich S, Dikin DA, Piner RD, Kohlhaas KA, Kleinhammes A, Jia Y, Wu Y, Nguyen ST, Ruoff RS. **Synthesis of Graphene-Based Nanosheets via Chemical Reduction of Exfoliated Graphite Oxide.** *Carbon* 2007; **45**(7): 1558-1565.

[49] Alswata AA, Ahmad MB, Al-Hada NM, Kamari B, Hussein MZ. **Preparation of Zeolite/Zinc Oxide Nanocomposites for Toxic Metals Removal from Water.** *Results in Physics* 2017; **7**: 723-731.

[50] Hellal MS, El-Sebaie SZ, Abou-Taleb EM, El-Khatib AM. **Adsorption Characteristics of Nickel (II) from Aqueous Solutions by Zeolite Scony Mobile-5 (ZSM-5) Incorporated in Sodium Alginate Beads.** *Scientific Reports* 2023; **13**(1): 19601.

[51] Alswata AA, Ahmad MB, Al-Hada NM, Kamari B, Hussein MZ. **Preparation of Zeolite/Zinc Oxide Nanocomposites for Toxic Metals.** 2017.

[52] Kadimpati KK, Mondal S, Sarda AB, Gidugu MS. **Entrapment of Marine Microalga, Isochrysis galbana, for Biosorption of Cr (III) from Aqueous Solution: Isotherms and Spectroscopic Characterization.** *Applied Water Science* 2013; **3**(1): 85-92.

[53] Naushad M, Alothman ZA, Islam M, Khan MR, Al-Shehri SM. **Removal of BrO 3– from Drinking Water Samples Using Newly Developed Agricultural Waste-Based Activated Carbon and Its Determination by Ultra-Performance Liquid Chromatography-Mass Spectrometry.** *Environmental Science and Pollution Research* 2015; **22**: 15853-15865.

[54] Mirzababaei SN, Taghizadeh M, Alizadeh E. **Synthesis of Surfactant-Modified ZSM-5 Nanozeolite for the Removal of Nickel (II) from Aqueous Solution.** *Desalination and Water Treatment* 2016; **57**(26): 12204-12215.

[55] Jin T, Li J, Geng J, Zhou Y. **Adsorption Thermodynamics and Kinetics of Nickel (II) Ions onto Na-ZSM-5 and Mordenite Zeolites.** *International Journal of Environmental Engineering* 2009; **1**(3): 321-333.